

# Chapter 7

## Effective Diffusion Coefficient of a Porous Material Applied to the Problem of Hydrogen Damage



Ksenia P. Frolova and Elena N. Vilchevskaya

**Abstract** The chapter focuses on calculation of the effective diffusion coefficient of a porous material accounting for the volume fraction, shape of pores, and their distribution over orientations in a three-dimensional solid. The existing pores are considered as embedded inhomogeneities possessing a high diffusivity in comparison with a matrix. The segregation effect is taken into account. Maxwell homogenization schemes in terms of diffusivity and resistivity contribution tensors are used. Inhomogeneities are assumed to have a spheroidal shape. The paper considers diverse microstructural patterns, namely, (1) arbitrary orientation distribution of pores, (2) orientational scatter of pores about a preferential orientation, (3) arbitrary orientation distribution of rotational axes of spheroidal pores in one plane. Application of the model to problems related to hydrogen damage is discussed.

**Keywords** Effective diffusivity · Homogenization problem · Maxwell scheme · Segregation effect

### 7.1 Introduction

Correct estimation of the value of the diffusion coefficient allows one to predict the amount of hydrogen in metals and alloys. Increasing the amount of hydrogen, in turn, may lead to a premature failure of structural elements of metal parts [1, 2]. Determination of the effective diffusion coefficient of a porous material is of practical interest, since voids and microcracks are known to be traps for hydrogen [3, 4].

---

K. P. Frolova (✉) · E. N. Vilchevskaya  
Institute for Problems in Mechanical Engineering RAS, Bolshoy pr., 61, V.O., 199178  
St. Petersburg, Russia  
e-mail: [kspfrolova@gmail.com](mailto:kspfrolova@gmail.com)

E. N. Vilchevskaya  
e-mail: [vilchevska@gmail.com](mailto:vilchevska@gmail.com)

Diffusion of hydrogen in materials containing microcracks and discontinuities formed during manufacture can be observed in sacrificial coatings that are used to protect steel against corrosion [5, 6]. Among other reasons, permeability of coatings is determined by its microstructure. In [5], it was shown that Zn–Ni coatings can contain through-thickness defects that makes the steel exposed to hydrogen uptake. Correlation between the diffusion coefficient and the microstructural characteristics of Zn–Ni and Cd coatings was investigated in [6]. Thus, it is of quite importance to predict permeability of materials containing pores emerged before hydrogenation.

Numerous papers are devoted to investigation of microstructure of materials affected by hydrogen [1, 7–11]. It is believed that hydrogen diffuses through metals and alloys lattice and accumulates within structural defects such as dislocations, pores, and vacancies leading to initiation and propagation of hydrogen-stimulated microcracks. Typically, defects are occurring at grain boundaries or inclusions due to manufacturing. Thus, in the absence of the inner and outer stresses, hydrogen-induced cracking is observed to take place mainly along grain boundaries [1, 7, 9]. Two types of intergranular cracking can be found in material, namely, void formation along grain boundaries and grain boundary triple junction cracking [1, 7, 10, 11]. Also, hydrogen charging may lead to blistering of the surface [8, 11]. The hydrogen-induced cracks are oriented primarily along the rolling direction of steel [8, 9]. Hydrogen-induced defects may, in turn, increase permeability of a material right during hydrogenation.

The focus is usually set on diffusion of hydrogen along grain boundaries while investigating the effect of presence of high diffusivity paths in metals. To the best of our knowledge, the earliest quantitative model for a diffusion in a heterogeneous material accounting for a single rectilinear grain boundary embedded in a semi-infinite solid of much lower diffusivity was proposed in [12] for the problem of self-diffusion of silver. The same geometry with less restrictive boundary conditions has been considered in [13, 14]. Lamellar and columnar microstructures were modeled in [15], where the obtained expressions were similar to Wiener bounds for thermal or electrical conductivity [16]. The fact that the grain boundaries completely surround grains in a three-dimensionally interconnected network, and are not simply distributed in parallel, has been addressed by numerous diffusion models that embedded grains in a matrix representing grain boundaries [17, 18]. A rule of mixture was used in [19] to calculate the effective diffusion coefficient. A number of approximate schemes accounting for the interactions between inhomogeneities were rewritten in [20] for diffusivity on the base of similarity between governing equations in the diffusivity and conductivity problems. However, a principal difference between two problems is that temperature is a continuous function across the phase boundaries, while concentration is usually not. Therefore, the segregation effect should be taken into account [21]. Hart and Maxwell–Garnett equations were rewritten in the form containing the segregation factor in [22, 23]. The results may be employed for description of materials containing spherical grains. Typical micromechanical models were rewritten for diffusivity in [24] to calculate the effective diffusion coefficient of a polycrystalline material accounting for the isotropic distribution of spheroidal grains over orientation. A similar problem was solved in [25] numerically.

The present paper is concerned with a quantitative characterization of mass transport process in a porous material. Such a microstructural pattern is corresponding to a composite material consisting of grains, grain boundaries, various defects, and isolated pores. Hydrogen is assumed to diffuse along grain boundaries and fill the pores. A composite consisting of grains, grain boundaries, and various defects is represented by a homogenized background matrix with a known effective diffusivity. Pores are considered as embedded inhomogeneities.

The effect of oblate and prolate spheroidal pores, as well as spherical ones, is investigated. An oblate spheroidal pore models a hydrogen-stimulated microcrack occurring between two grains. A prolate spheroidal inhomogeneity reflects the influence of an intragranular microcrack or microcrack propagating along a few grain boundaries. Such a microstructure can be observed in non-saturated materials like sacrificial coatings. Generally speaking, in this case, it is more correct to introduce an ellipsoidal inhomogeneity that is not considered within the frame of the present research. A spherical inhomogeneity models an isolated pore in the host material.

The paper accounts for different orientation distribution of inhomogeneities, namely,

- Arbitrary orientation distribution of pores specific for weakly deformable materials;
- Orientational scatter of pores about a preferential orientation specific for materials prepared by rolling;
- Arbitrary orientation distribution of rotational axes of spheroidal pores in one plane that can be observed for compressed materials.

All the mentioned cases are corresponding to the transversally isotropic porous material. The question arises, how the diffusion coefficient of a matrix material containing grains, grain boundaries, and various defects changes due to the presence of pores.

## 7.2 Problem Statement

In the present paper, we apply micromechanical approximate schemes to calculate effective diffusivity of a material containing isolated pores assuming that the matrix material (consisting of grains, grain boundaries, and various defects) is homogeneous. Thus, homogenization contains two steps. At the first implicit step, the effective properties of matrix material are obtained by means of experimental data [26] or theoretical framework [24]. At the second explicit step, the effective properties of a porous material are calculated (see Fig. 7.1).

To reflect the effect of pores on the effective properties of a heterogeneous material, we consider inhomogeneities with diffusion coefficient  $D_1$  in a solid of much lower diffusion coefficient  $D_0$ . The value  $D_1 \rightarrow \infty$  providing a zero ratio  $\alpha = D_0/D_1$  can be considered for simpleness. However, it is more correct to take into account a non-zero  $\alpha \ll 1$  to explain a real phenomenon. We assume that the value of the

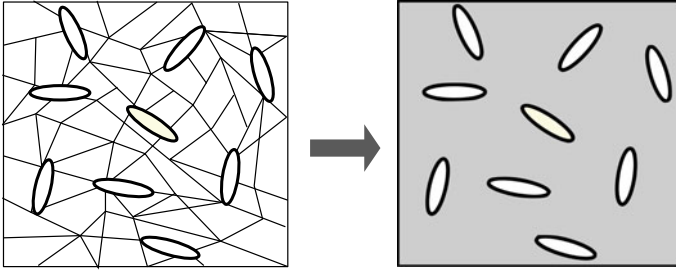


**Fig. 7.1** Schematic representation of the model

diffusion coefficient of pores is the same as for unfilled grain boundaries ( $D_1 = D_{GB}$ ). According to [27], the contrast in the diffusion coefficient of the bulk material of grains,  $D_B$ , and grain boundaries,  $D_{GB}$ , varies from 0.005 to 0.1. Knyazeva et al. [24] considered  $\tilde{\alpha} = D_B/D_{GB} = 0.015$ . The contrast in the effective diffusion coefficient of matrix,  $D_0$ , and bulk material of grains,  $D_B$ , increases with decreasing of the grain size [24, 26]. If the grain diameter is about 10 – 13  $\mu\text{m}$ , the value of  $\tilde{\alpha}_{eff} = D_0/D_B$  is equal to 2.2–4.4 [24, 26]. Then,

$$\alpha = \frac{D_0}{D_1} = \tilde{\alpha}_{eff}\tilde{\alpha}$$

takes values in the range 0.03–0.07. Within the frame of the present paper, we assume that  $\alpha = 0.05$ .

We assume continuity of the normal component of the solute flux across the matrix/pore interface and a constant jump in hydrogen concentration,  $c$ , described by the segregation factor,  $s$ , as follows:

$$c(x)|_{x \rightarrow \partial V_+} = sc(x)|_{x \rightarrow \partial V_-} \quad (7.1)$$

We are especially interested in cases when hydrogen is partially trapped inside the pores and, therefore, focus on cases  $s < 1$ . For completeness, we also consider the case when concentration is a continuous function across the phase boundaries and, therefore, there is no segregation effect ( $s = 1$ ). We assume that the segregation effect is independent of the type of pore. Also, segregation related to pore saturation is not discussed here.

The certain preferential orientation distribution of pores is described by means of the probability density function introduced by Sevostianov [28]:

$$\psi_\lambda(\theta) = \frac{1}{2\pi} [(\lambda^2 + 1)e^{-\lambda\theta} + \lambda e^{-\lambda\pi/2}]. \quad (7.2)$$

This probability density function is defined on the upper semisphere of unit radius ( $0 \leq \theta \leq \pi/2$ ) and subject to the normalization condition. The scatter parameter  $\lambda$

varies in the range from zero to infinity that corresponds to fully random and strictly parallel orientations of pores, respectively.

To obtain the explicit expressions for the effective properties, we use the formulation of Maxwell's homogenization scheme in terms of diffusivity (resistivity) contribution tensors [24, 29].

### 7.3 Diffusivity Contribution Tensors

Following [29, 30], we introduce property contribution tensors to express the effect of a given inhomogeneity on the properties of interest. Their sums are proper microstructural parameters that reflect contributions of individual inhomogeneities to the overall effective properties. To explain the process of mass transfer, we introduce the second-rank diffusivity and resistance contribution tensors,  $\mathbf{H}^D$  or  $\mathbf{H}^{DR}$ .

Let us consider a reference volume  $V$  of an infinite three-dimensional solid with the isotropic diffusivity tensor  $\mathbf{D}_0 = D_0 \mathbf{I}$  containing inhomogeneity with the isotropic diffusivity tensor  $\mathbf{D}_1 = D_1 \mathbf{I}$  occupying domain  $V_1 \ll V$ . We assume that both inhomogeneity and the surrounding material obey the linear Fick's law connecting the vector of molar flux with the concentration gradient. The extra molar flux due to the inhomogeneity is as follows:

$$\Delta \mathbf{J} = \frac{V_1}{V} \mathbf{H}^D \cdot \mathbf{G}_0, \quad (7.3)$$

where  $\mathbf{G}_0$  is a concentration gradient prescribed at the boundary of  $V$ . The diffusivity contribution tensor  $\mathbf{H}^D$  depends on the shape of the inhomogeneity, diffusivity contrast between inhomogeneity and surrounding material, and the segregation of particles at the interface.

Assuming continuity of the normal component of the solute flux across the matrix/inhomogeneity interface and a segregation effect described by Eq. (7.1), the diffusivity contribution tensor representing the contribution of the spheroidal inhomogeneity to the overall diffusivity of volume  $V$  can be written in the form [24]

$$\mathbf{H}^D = D_0 [B_1 (\mathbf{I} - \mathbf{nn}) + B_2 \mathbf{nn}], \quad (7.4)$$

where taking  $\alpha = D_0/D_1$ ,

$$B_1 = \frac{1 - \alpha}{s\alpha + (1 - s\alpha) f_0}, \quad B_2 = \frac{1 - \alpha}{1 - 2(1 - s\alpha) f_0}. \quad (7.5)$$

Shape function  $f_0 = f_0(\gamma)$  depends on the aspect ratio of the spheroidal inhomogeneity  $\gamma = a_3/a$  ( $a_3$  is the rotation axis,  $a_1 = a_2 = a$  are two other semiaxes) in the following way:

$$f_0 = \frac{1 - g}{2(1 - \gamma^{-2})}, \quad (7.6)$$

where

$$g = \begin{cases} \frac{1}{\gamma\sqrt{1-\gamma^2}} \arctan \frac{\sqrt{1-\gamma^2}}{\gamma}, & \gamma \leq 1 \\ \frac{1}{2\gamma\sqrt{\gamma^2-1}} \ln \left( \frac{\gamma + \sqrt{\gamma^2-1}}{\gamma - \sqrt{\gamma^2-1}} \right), & \gamma \geq 1. \end{cases} \quad (7.7)$$

The diffusion resistance contribution tensor  $\mathbf{H}^{DR}$  that is dual to  $\mathbf{H}^D$  can be introduced in a similar way. It appears if, instead of uniform gradient of concentration, a uniform molar flux is remotely applied. Tensors  $\mathbf{H}^{DR}$  and  $\mathbf{H}^D$  interrelate as follows [24]:

$$\mathbf{H}^{DR} = -\frac{1}{D_0^2} \mathbf{H}^D. \quad (7.8)$$

According to [29], there are no any explicit evidence regarding preference of one of tensor  $\mathbf{H}^{DR}$  or  $\mathbf{H}^D$ . So, it is necessary to check which one of these tensors yields better agreement with experimental data.

Note that according to Eqs. (7.4) and (7.5), the segregation factor  $s$  does not play any role and simplifies the model in the case when  $\alpha \rightarrow 0$  due to  $D_1 \rightarrow \infty$ .

## 7.4 Homogenization Problem

An exact solution of the homogenization problem for a composite material with multiple inhomogeneities can be obtained only numerically. Moreover, specific materials with a known microstructure should be considered. All analytical approximation methods involve uncertainties and/or inconsistencies. A detailed review of history of various methods can be found in [31], whereas the current state of knowledge of the problem is described in [29].

We use the Maxwell homogenization scheme, since it appears to be one of the best schemes, in terms of its applicability to cases of multiphase composites and accuracy. In his original work, Maxwell addressed the problem of effective electrical conductivity of a material containing multiple spherical inhomogeneities [32]. The accuracy of Maxwell's original formula was checked by means of a periodic array of spheres and found to be accurate up to volume fractions about 40% [33]. We use the formulation of Maxwell scheme in terms of property contribution tensors proposed in [28, 34].

According to Maxwell's idea, it is necessary to evaluate far-field perturbations due to inhomogeneities in two different ways and equate the results. The first way is to evaluate this field as the one generated by a homogenized region  $\Omega$  possessing the (yet

unknown) effective properties. This field can be expressed in terms of the property contribution tensor of the domain  $\Omega$ . The second way is based on consideration the sum of far fields generated by all the individual inhomogeneities within  $\Omega$  (treated as non-interacting ones). Equating the results yields the effective diffusion properties in the form [24]

$$(\mathbf{D}^{eff})^{-1} = \frac{1}{D_0} \mathbf{I} + \left\{ \left[ \frac{1}{V_\Omega} \sum_k V_k \mathbf{H}_k^{DR} \right]^{-1} - \mathbf{Q}_\Omega^D \right\}^{-1} \quad (7.9)$$

in terms of the resistivity and

$$\mathbf{D}^{eff} = D_0 \mathbf{I} + \left\{ \left[ \frac{1}{V_\Omega} \sum_k V_k \mathbf{H}_k^D \right]^{-1} - \mathbf{P}_\Omega^D \right\}^{-1} \quad (7.10)$$

in terms of diffusivity. Here,

$$\mathbf{Q}_\Omega^D = D_0 s_\Omega [(1 - f_0(\gamma_\Omega^D)) (\mathbf{I} - \mathbf{m}\mathbf{m}) + 2f_0(\gamma_\Omega^D) \mathbf{m}\mathbf{m}], \quad (7.11)$$

$$\mathbf{P}_\Omega^D = \frac{1}{D_0 s_\Omega} [f_0(\gamma_\Omega^D) (\mathbf{I} - \mathbf{m}\mathbf{m}) + (1 - 2f_0(\gamma_\Omega^D)) \mathbf{m}\mathbf{m}] \quad (7.12)$$

are the second-rank Hill's tensors that reflect the shape of spheroidal domain  $\Omega$  and take into account interactions between the inhomogeneities. Vector  $\mathbf{m}$  is supposed to be a unit vector along the axis of symmetry of the domain  $\Omega$ . Note that  $\mathbf{n}$  is corresponding to the axis of symmetry of individual spheroidal inhomogeneity and, therefore,  $\mathbf{m}$  may not coincidence with  $\mathbf{n}$ .

The segregation factor  $s_\Omega$  describes a constant jump in the particles concentration at the interface between the domain  $\Omega$  and matrix. This segregation factor can not be estimated experimentally in contrast to the segregation factor for the matrix/inhomogeneity interface. In [35, 36], these parameters were supposed to be equal. Results obtained at  $s_\Omega = s$  and  $s_\Omega = 1$  were compared with the experimental data for a polycrystalline material in [24]. It was shown that  $s_\Omega = 1$  does not provide correct values of the effective diffusion coefficient at large values of the volume fraction of inhomogeneities. At the same time, value of  $s_\Omega$  does not play a role at small values of the volume fraction of inhomogeneities.

Recommendations regarding the choice of the shape of the domain  $\Omega$  can be found in [28]. This shape has to obey the following requirements: (1) it should be ellipsoidal, (2) it should properly reflect the shapes of individual inhomogeneities, their orientations and properties. Within the frame of the present paper, we consider materials with transversely isotropic microstructure. In this case, the domain  $\Omega$  is a spheroid. In the specific case of random orientation distribution of inhomogeneities, the shape of the domain is spherical ( $\gamma_\Omega = 1$ ). In the case of preferentially oriented inhomogeneities, following [28], we introduce the shape of the domain  $\Omega$  as

$$\gamma_{\Omega}^D = \frac{\sum_k V_k P_{11}^D}{\sum_k V_k P_{33}^D}, \quad (7.13)$$

where  $P_{11}$ ,  $P_{33}$  are components of the second-rank Hill's tensor

$$\mathbf{P}^D = \frac{1}{D_0 s} [f_0(\gamma) (\mathbf{I} - \mathbf{nn}) + (1 - 2f_0(\gamma)) \mathbf{nn}] \quad (7.14)$$

for individual spheroidal inhomogeneity.

The effective properties of a considered material with pores of identical shapes and size and diverse distribution over their orientations can be expressed in terms of their volume fraction  $\phi = \sum_k V_k / V$  [29]. Summation in Eqs. (7.9), (7.10), and (7.13) can be replaced by multiplication of the fraction volume by averaged tensors, so

$$\frac{1}{V} \sum_k V_k \mathbf{H}^D = \phi \langle \mathbf{H}^D \rangle, \quad \frac{1}{V} \sum_k V_k \mathbf{H}^{DR} = \phi \langle \mathbf{H}^{DR} \rangle,$$

$$\frac{1}{V} \sum_k V_k \mathbf{P}^D = \phi \langle \mathbf{P}^D \rangle.$$

The tensor averaging is equivalent to averaging of dyads  $\mathbf{nn}$ , since these tensors are determined by means of  $\mathbf{nn}$  and  $\mathbf{I} - \mathbf{nn}$ .

We first consider orientation distribution of  $\mathbf{n}$  about a preferential orientation  $\mathbf{m}$  accompanied by a random scatter. This orientation distribution of pores is described by Eq. (7.2). The averaging of the dyad  $\mathbf{nn}$  can be obtained by integration over the upper semisphere of unit radius  $\tilde{\Omega}_{1/2}$ , so

$$\langle \mathbf{nn} \rangle = \int_{\tilde{\Omega}_{1/2}} (\mathbf{nn})_k \psi_{\lambda} d\tilde{\Omega}_{1/2}.$$

Then,

$$\langle \mathbf{nn} \rangle = g_1 \boldsymbol{\theta} + g_2 \mathbf{mm},$$

where  $\boldsymbol{\theta} = \mathbf{I} - \mathbf{mm}$  and

$$g_1 = \frac{18 - e^{-\frac{\pi\lambda}{2}} \lambda (3 + \lambda^2)}{6(9 + \lambda^2)}, \quad g_2 = \frac{(3 + e^{-\frac{\pi\lambda}{2}} \lambda)(3 + \lambda^2)}{3(9 + \lambda^2)}.$$

Equations (7.9), (7.10) reduce to



$$\frac{\mathbf{D}^{eff}}{D_0} = \frac{1}{1 - \left[ \frac{1}{\phi(B_1(1-g_1)+B_2g_1)} + s_\Omega (1 - f_0(\gamma_\Omega^D)) \right]^{-1}} \boldsymbol{\theta} + \frac{1}{1 - \left[ \frac{1}{\phi(B_1(1-g_2)+B_2g_2)} + 2s_\Omega f_0(\gamma_\Omega^D) \right]^{-1}} \mathbf{mm}, \quad (7.15)$$

$$\frac{\mathbf{D}^{eff}}{D_0} = \left( 1 + \left[ \frac{1}{\phi(B_1(1-g_1)+B_2g_1)} - \frac{f_0(\gamma_\Omega^D)}{s_\Omega} \right]^{-1} \right) \boldsymbol{\theta} + \left( 1 + \left[ \frac{1}{\phi(B_1(1-g_2)+B_2g_2)} - \frac{(1-2f_0(\gamma_\Omega^D))}{s_\Omega} \right]^{-1} \right) \mathbf{mm}. \quad (7.16)$$

In the case of arbitrary orientation distribution of inhomogeneities  $\lambda = 0$  and, therefore,

$$\langle \mathbf{nn} \rangle = \frac{1}{3} \mathbf{I}$$

and Eqs. (7.9), (7.10) take forms

$$\frac{D^{eff}}{D_0} = \frac{3 + 2\phi\eta s_\Omega}{3 + \phi\eta(2s_\Omega - 3)}, \quad (7.17)$$

$$\frac{D^{eff}}{D_0} = \frac{3s_\Omega + \phi\eta(3s_\Omega - 1)}{3s_\Omega - \phi\eta}, \quad (7.18)$$

where  $\eta = \eta(\gamma, \alpha, s) = 2B_1/3 + B_2/3$ .

Now, turn to the case of random orientation distribution of unit vectors  $\mathbf{n}$  in the plane normal to unit vector  $\mathbf{m}$ . The averaging of the dyad  $\mathbf{nn}$  can be obtained by integration over a circle of unit radius  $l_1$  normal to  $\mathbf{m}$ , so

$$\langle \mathbf{nn} \rangle = \frac{1}{2\pi} \int_{l_1} (\mathbf{nn})_k dl_1.$$

Therefore,

$$\langle \mathbf{nn} \rangle = \frac{1}{2} \boldsymbol{\theta}$$

and Eqs. (7.9), (7.10) reduce to

$$\frac{\mathbf{D}^{eff}}{D_0} = \frac{1}{1 - \left[ \frac{2}{\phi(B_1+B_2)} + s_\Omega (1 - f_0(\gamma_\Omega^D)) \right]^{-1}} \boldsymbol{\theta} + \frac{1}{1 - \left[ \frac{1}{\phi B_1} + 2s_\Omega f_0(\gamma_\Omega^D) \right]^{-1}} \mathbf{mm}, \quad (7.19)$$

$$\frac{\mathbf{D}^{eff}}{D_0} = \left( 1 + \left[ \frac{2}{\phi(B_1+B_2)} - \frac{f_0(\gamma_\Omega^D)}{s_\Omega} \right]^{-1} \right) \boldsymbol{\theta} + \left( 1 + \left[ \frac{1}{\phi B_1} - \frac{1 - 2f_0(\gamma_\Omega^D)}{s_\Omega} \right]^{-1} \right) \mathbf{mm}. \quad (7.20)$$

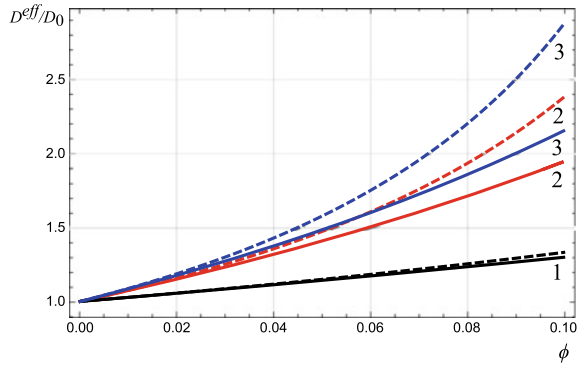
According to [34], Maxwell's scheme formulated in terms of diffusivity and resistivity contribution tensors should lead to the same result. Any contradictions may cause incorrect accounting for interactions between inhomogeneities within the scheme. Comparing the results obtained within the present section in terms of diffusivity and resistivity contribution tensors, one can see that the equality of two solutions imposes restrictions on the segregation factor  $s_\Omega$  for the interface between the domain  $\Omega$  and matrix. Maxwell's scheme formulated in terms of diffusivity and resistivity contribution tensors for the considered cases of the orientation distribution of inhomogeneities leads to the same result only at certain values of the segregation factor  $s_\Omega$ . In particular, effective properties obtained within Maxwell's scheme formulated in terms of diffusivity and resistivity contribution tensors are the same in all the mentioned cases of the orientation pattern when the segregation factor  $s_\Omega = 1$  that means that there is no segregation effect at the interface domain  $\Omega$ /matrix. In the case of random distribution of the inhomogeneities, the segregation factor  $s_\Omega$  can also be equal to 0.5. In the cases of preferentially oriented inhomogeneities, accounting for the segregation effect leads to incorrect results.

## 7.5 Effective Diffusion Coefficient of a Material with Spheroidal Pores

The effective diffusion coefficient of a material containing pores depends on the shape of the inhomogeneities, its volume fraction and distribution over orientations, as well as on the segregation effect. We now investigate these dependences for a heterogeneous material described in Sect. 7.2. Thus, we consider  $\alpha = D_0/D_1 = 0.05$  and  $s \leq 1$ .

We start with modeling of an isotropic distribution of spheroidal inhomogeneities. The accuracy of Maxwell's scheme was found to be determined by volume fraction of

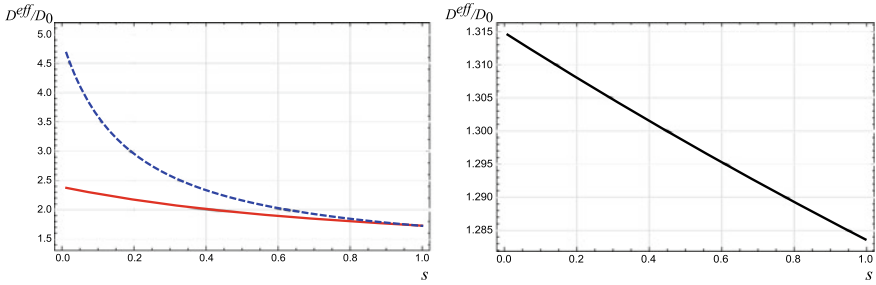
**Fig. 7.2** Dependences of the effective diffusion coefficient on the volume fraction of (1) spherical pores, (2) oblate spheroidal pores with  $\gamma = 0.1$ , (3) prolate spheroidal pores with  $\gamma = 10$  at  $s_\Omega = 1$  (solid line) and  $s_\Omega = 0.5$  (dashed line); case of random orientation distribution of pores



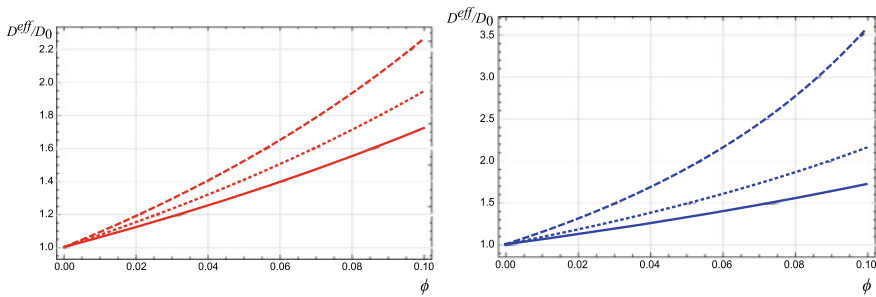
pores. Such a restriction was discussed in our paper [37] for the case of material containing oblate spheroidal pores. Figure 7.2 illustrates dependences of the normalized effective diffusion coefficient,  $D^{eff}/D_0$ , on the volume fraction of pores,  $\phi$ , at two different values of the segregation factor for the interface between the inhomogeneity with effective properties occupying domain  $\Omega$  and matrix ( $s_\Omega = 1$  and  $s_\Omega = 0.5$ ). Segregation at the interface between an isolated inhomogeneity and matrix is determined by a fixed value  $s = 0.5$ . Accounting for the segregation effect at the interface domain  $\Omega$ /matrix ( $s_\Omega \neq 1$ ) increases the effective diffusion coefficient. Additional efforts are needed to check whether accounting for segregation effect at the interface domain  $\Omega$ /matrix in the model yields better agreement with the experimental data. Hereafter, we assume that  $s_\Omega = 1$ .

Figure 7.3 illustrates dependences of the normalized effective diffusion coefficient on the segregation factor at the interface inhomogeneity/matrix at a constant volume fraction  $\phi = 0.1$ . According to the results, decreasing the segregation factor  $s$  increases the effective diffusion coefficient and vice versa. The ratio  $D^{eff}/D_0$  is minimal when there is no segregation effect ( $s = 1$ ). Thus, segregation of particles inside pores produces effect similar to increasing diffusivity of an inhomogeneity. At the same time, it is seen that the segregation of particles inside spherical pores does not change the effective diffusion coefficient significantly. Thus, segregation inside pores increases the effect of shape of the inhomogeneities on the overall diffusion coefficient. Figure 7.4 demonstrates that accounting for segregation of particles inside non-spherical pores at high volume fractions of pores is of great importance. Figure 7.5 illustrates the effect of shape on the effective diffusion coefficient at  $\phi = 0.1$  and  $s = 0.5$ .

Consider now material containing spheroidal pores that have mild tendency to be parallel to each other. Dependences of the effective diffusion coefficients on the scatter parameter are shown in Fig. 7.6. Increasing of the scatter parameter  $\lambda$ , i.e., decreasing of randomness of the orientation distribution, leads to increasing of the effective diffusion coefficient within the plane of isotropy of a material containing oblate spheroidal pores with  $\gamma = 0.1$  and to decreasing of its effective diffusion coefficient along the axis of symmetry. In the case of prolate spheroidal pores with

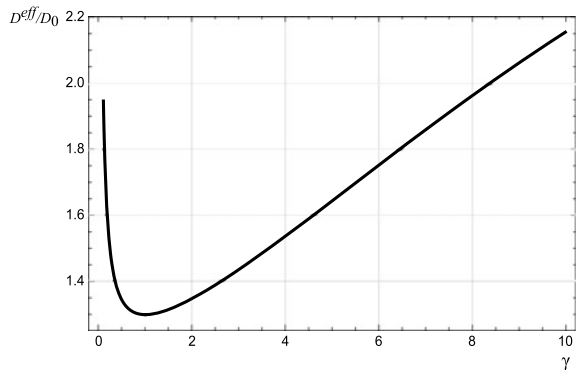


**Fig. 7.3** Dependences of the effective diffusion coefficient of a material containing non-spherical pores (left-hand side), namely, oblate spheroidal pores with  $\gamma = 0.1$  (solid line) and prolate spheroidal pores with  $\gamma = 10$  (dashed line), and spherical pores (right-hand side) on the segregation factor  $s$ ; case of random orientation distribution of pores



**Fig. 7.4** Dependences of the effective diffusion coefficient on the volume fraction of oblate pores with  $\gamma = 0.1$  (left-hand side) and prolate pores with  $\gamma = 10$  (right-hand side) at  $s = 0.1$  (dashed line),  $s = 0.5$  (dotted line) and  $s = 1$  (solid line); case of random orientation distribution of pores

**Fig. 7.5** Dependence of the effective diffusion coefficient on the aspect ratio of pores in the case of random orientation distribution of inhomogeneities



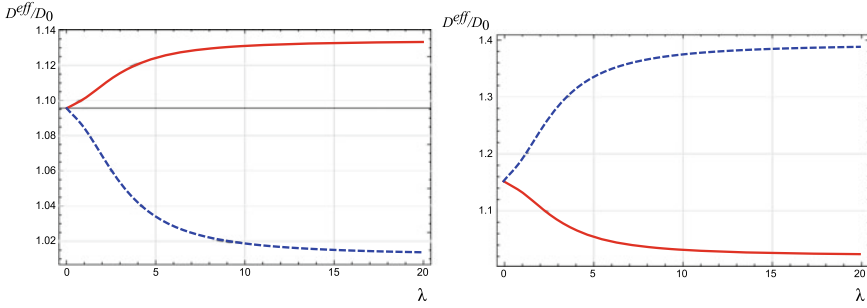


**Fig. 7.6** Dependences of the effective diffusion coefficients  $D_{11}^{eff}/D_0$  (solid line) and  $D_{33}^{eff}/D_0$  (dashed line) of a material with oblate spheroidal pores with  $\gamma = 0.1$  (left-hand side) and material with prolate spheroidal pores with  $\gamma = 10$  (right-hand side) on lambda; case of certain preferential orientation accompanied by random scatter

$\gamma = 10$ , it is the other way round. We take  $\phi = 0.01$  and  $s = 0.5$ . Note that the qualitative result will be similar if we use other values of the aspect ratios, volume fraction, and segregation factor.

The oblate spheroidal pores were found to change diffusion within the plane of isotropy and to have no significant influence on the value of the diffusion coefficient along the axis of symmetry. The situation was found to be opposite in the case of prolate spheroids. Figure 7.7 illustrates dependences of the normalized effective diffusion coefficient on the segregation factor at the interface inhomogeneity/matrix at a constant volume fraction  $\phi = 0.1$  and scatter parameter  $\lambda = 20$ . For the sake of brevity, we do not provide dependences  $D_{33}^{eff}/D_0$  on  $s$  corresponding to a material with oblate pores and  $D_{11}^{eff}/D_0$  on  $s$  corresponding to a material with prolate pores, since these effective diffusion coefficients are weakly dependent on the segregation effect in the mentioned cases due to the weak effect of shape. As in the case of random distribution, segregation inside pores increases effect of shape on the overall diffusion coefficient. Figure 7.8 illustrates the effect of shape on the effective diffusion coefficient at  $\phi = 0.1$ ,  $s = 0.5$  and  $\lambda = 20$ .

Finally, turn to the problem of random orientations of unit vectors  $\mathbf{n}$  in one plane. The oblate spheroidal pores were found to change diffusion within the plane of isotropy and along the axis of symmetry, whereas prolate spheroidal pores were found to influence only diffusivity within the plane of isotropy. Again, for the sake of brevity, we do not provide dependence  $D_{33}^{eff}/D_0$  on  $s$  corresponding to a material with prolate pores, since this effective diffusion coefficient weakly depends on the segregation effect in the mentioned case due to the weak effect of shape. Figure 7.9 illustrates dependences of the normalized effective diffusion coefficient on the segregation factor at the interface inhomogeneity/matrix at a constant volume fraction  $\phi = 0.1$ . It is seen that segregation inside pores increases the effect of shape on the overall diffusion coefficient. Figure 7.10 illustrates the effect of shape on the effective diffusion coefficient.

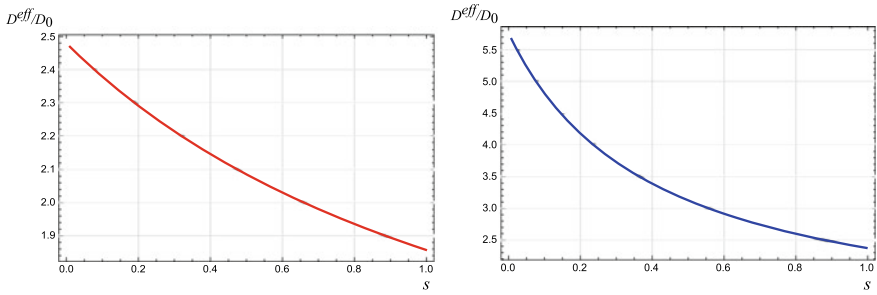


**Fig. 7.7** Dependences of the effective diffusion coefficients  $D_{11}^{eff}/D_0$  of a material with oblate spheroidal pores with  $\gamma = 0.1$  (left-hand side) and  $D_{33}^{eff}/D_0$  of a material with prolate spheroidal pores with  $\gamma = 10$  (right-hand side); case of certain preferential orientation accompanied by a random scatter ( $\lambda = 20$ )

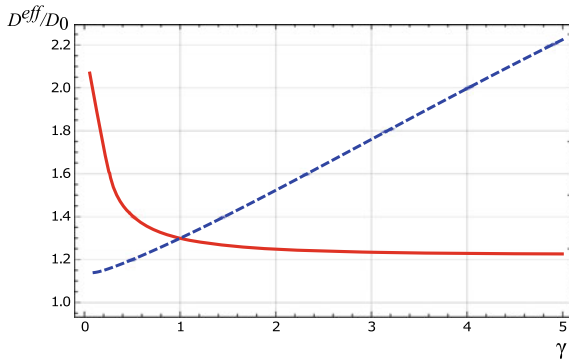


**Fig. 7.8** Dependences of the effective diffusion coefficients  $D_{11}^{eff}/D_0$  (solid line) and  $D_{33}^{eff}/D_0$  (dashed line) on the aspect ratio of pores in the case of their certain preferential orientation accompanied by a random scatter ( $\lambda = 20$ )

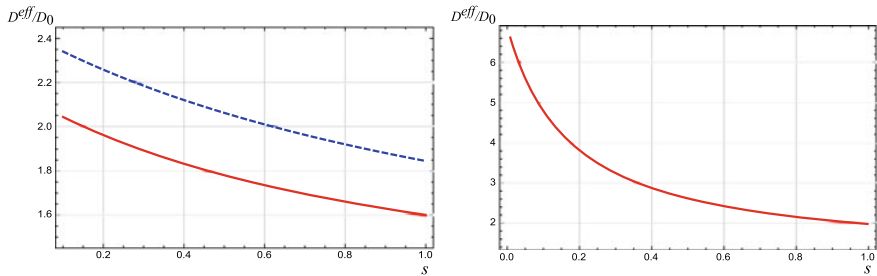
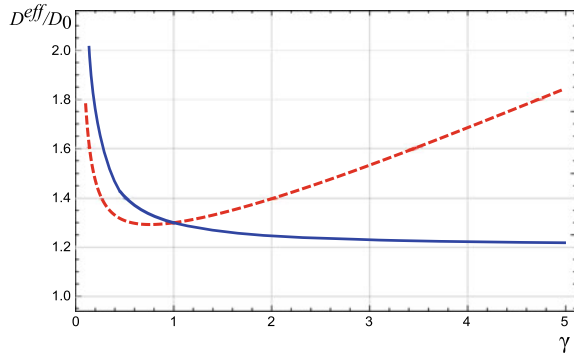


**Fig. 7.9** Dependences of the effective diffusion coefficients  $D_{11}^{eff}/D_0$  (solid line) and  $D_{33}^{eff}/D_0$  (dashed line) of a material containing oblate spheroidal pores with  $\gamma = 0.1$  (left-hand side) and prolate spheroidal pores with  $\gamma = 10$  (right-hand side) on the segregation factor  $s$ ; case of random orientations of unit vectors  $\mathbf{n}$  in one plane

**Fig. 7.10** Dependences of the effective diffusion coefficients  $D_{11}^{eff}/D_0$  (dashed line) and  $D_{33}^{eff}/D_0$  (solid line) on the aspect ratio of pores in the case of random orientations of unit vectors  $\mathbf{n}$  in one plane



Thus, it was shown that the presence of multiple pores of diverse shape and distribution over orientation can lead to a significant increase in the diffusion coefficient. The effect of shape was found to be strongly coupled with the distribution of inhomogeneities over orientation. In particular, diffusion coefficients in diverse directions can be changed in various ways with respect to the shape of a non-spherical pore. The segregation of hydrogen at the interface matrix/pore was found to have a significant effect on the effective diffusivity, especially in the case of preferentially oriented prolate pores.

## 7.6 Description of the Experimental Data by Means of the Proposed Model

To illustrate the applicability of the results of modeling to problems associated with hydrogen damage, we describe results obtained in [6]. Authors of [6] analyzed the permeability of Zn–Ni coating material to hydrogen in correlation with its microstructural characteristics. In particular, they indicated that Zn–Ni coatings typically exhibit defects, such as intergranular cracks and through-thickness pores. Changing of a substrate geometry during the permeability test realized by the twin cell method led to changing of the microcracks distribution in the coatings. As a result, microcracks were found to be randomly distributed. The microstructure of coatings with and without defects was shown in Scanning Electron Microscope (SEM) images. Initiated defects may make coatings susceptible to environmental hydrogen embrittlement. Authors compared the hydrogen diffusion coefficients corresponding to uniform coating and coating with defects. The ratio of the effective diffusion coefficient to the diffusion coefficient of a host material is given in Table 7.1.

Unfortunately, there are no data on the exact shape and volume fraction of the defects. On the base of the SEM images shown in [6], we could say that microcracks appearing in Zn–Ni coating can be considered as prolate spheroidal pores that have certain preferential orientation ( $\lambda = 20$ ). Taking diverse realistic values of  $\gamma$  and

**Table 7.1** Correlation of the effective diffusion coefficient  $D^{eff}/D_0$  with its microstructural characteristics, namely, shape (by means of  $\gamma$ ), porosity ( $\phi$ ), and distribution over orientations

Experimental $D^{eff}/D_0$	$\gamma$ (fixed)	$\phi$ (range of values)	Distribution over orientations	Calculated $D^{eff}/D_0$
14.8 (Zn-Ni)	20	0.10–0.50	Certain preferential orientation ( $\lambda = 20$ )	4.70–19.75
	100	0.10–0.50		3.99 – 16.43

varying the value of the volume fraction, we can obtain a proper range of the effective diffusion coefficient. The results are shown in Table 7.1. We use  $s = 0.5$ ,  $s_\Omega = 1$ .

The suggested homogenization model leads to results that are in a good agreement with experimental data and, therefore, may be applied to estimate the effective diffusion coefficients of hydrogen in a porous material in the annex to the problem of hydrogen damage.

## 7.7 Conclusions

The paper addresses the effective diffusion properties of a porous material. The microstructure may comprise a mixture of inhomogeneities of diverse shapes and orientations. We assume that oblate pores can model hydrogen-induced intergranular microcracks, whereas prolate pores can model microcracks originating during processing and affecting further hydrogenation. The segregation of hydrogen inside pores takes place.

Maxwell scheme formulated in terms of property contribution tensors was applied to solve the homogenization problem. It was shown that the presence of pores can lead to a significant increase in the diffusion coefficient. Effect of shape and segregation effect was observed. The homogenization problem was solved at diverse distribution of inhomogeneities over orientations. The effect of shape was found to be coupled with the orientation distribution.

**Acknowledgements** This study was supported by the Russian Foundation for Basic Research (projects No. 20-08-01100, 18-08-00201).

## References

1. Koyama, M., Akiyama, E., Tsuzak, K.: Hydrogen-induced delayed fracture of a Fe–22Mn–0.6 C steel pre-strained at different strain rates. *Scripta Mater.* **66**(11), 947–950 (2012)
2. So, K.H., Kim, J.S., Chun, Y.S., Park, K.T., Lee, Y.K., Lee, C.S.: Hydrogen delayed fracture properties and internal hydrogen behavior of a Fe–18Mn–1.5 Al–0.6 C TWIP steel. *ISIJ Int.* **49**(12), 1952–1959 (2009)



3. Nair, S.V., Jensen, R.R., Tien, J.K.: Kinetic enrichment of hydrogen at interfaces and voids by dislocation sweep-in of hydrogen. *Metall. Trans. A* **14**(2), 385–393 (1983)
4. Pressouyre, G.M.: A classification of hydrogen traps in steel. *Metall. Trans. A* **10**(10), 1571–1573 (1979)
5. Figueroa, D., Robinson, M.J.: The effects of sacrificial coatings on hydrogen embrittlement and re-embrittlement of ultra high strength steels. *Corros. Sci.* **50**(4), 1066–1079 (2008)
6. Sriraman, K.R., Brahimi, S., Szpunar, J.A., Yue, S.: Hydrogen embrittlement of Zn-, Zn-Ni-, and Cd-coated high strength steel. *J. Appl. Electrochem.* **43**(4), 441–451 (2013)
7. Kuhr, B., Farkas, D., Robertson, I.M.: Atomistic studies of hydrogen effects on grain boundary structure and deformation response in FCC Ni. *Comput. Mater. Sci.* **122**, 92–101 (2016)
8. Merson, E.D., Myagkikh, P.N., Klevtsov, G.V., Merson, D.L., Vinogradov, A.: Effect of fracture mode on acoustic emission behavior in the hydrogen embrittled low-alloy steel. *Eng. Fract. Mech.* **210**, 342–357 (2019)
9. Shen, C.H., Shewmon, P.G.: A mechanism for hydrogen-induced intergranular stress corrosion cracking in alloy 600. *Metall. Trans. A* **21**(5), 1261–1271 (1990)
10. Sun, B., Krieger, W., Rohwerder, M., Ponge, D., Raabe, D.: Dependence of hydrogen embrittlement mechanisms on microstructure-driven hydrogen distribution in medium Mn steels. *Acta Mater.* **183**, 313–328 (2020)
11. Wasim, M., Djukic, M.B.: Hydrogen embrittlement of low carbon structural steel at macro-, micro- and nano-levels. *Int. J. Hydrogen Energy* **45**(3), 2145–2156 (2020)
12. Fisher, J.C.: Calculation of diffusion penetration curves for surface and grain boundary diffusion. *J. Appl. Phys.* **22**(11), 74–77 (1951)
13. Le Claire, A.D.: The analysis of grain boundary diffusion measurements. *Br. J. Appl. Phys.* **14**(6), 351 (1963)
14. Suzuoka, T.: Exact solutions of two ideal cases in grain boundary diffusion problem and the application to sectioning method. *J. Phys. Soc. Jpn* **19**(6), 839–851 (1964)
15. Gilmer, G.H., Farrell, H.H.: Grain-boundary diffusion in thin films: I. The isolated grain boundary. *J. Appl. Phys.* **47**(9), 3792–3798 (1976)
16. Wiener, O.: *Abhandl. math.-phys. Kl. Königl. Sachsichen Gesell* **32**, 509 (1912)
17. Chen, Y., Schuh, C.A.: Geometric considerations for diffusion in polycrystalline solids. *J. Appl. Phys.* **101**(6), 063524 (2007)
18. Preis, W., Sitte, W.: Surface exchange reactions and fast grain boundary diffusion in polycrystalline materials: Application of a spherical grain model. *J. Phys. Chem. Solids* **66**(10), 1820–1827 (2005)
19. Hart, E.W.: Thermal conductivity. *Acta Metall.* **5**, 597–605 (1957)
20. Barrer, R.M.: Diffusion and permeation in heterogeneous media. *Diff. Poly.* **165–217** (1968)
21. Kaur, I., Mishin, Y., Gust, W.: *Fundamentals of Grain and Interphase Boundary Diffusion*. Wiley (1995)
22. Belova, I.V., Murch, G.E.: Diffusion in nanocrystalline materials. *J. Phys. Chem. Solids* **64**(5), 873–878 (2003)
23. Belova, I.V., Murch, G.E.: The effective diffusivity in polycrystalline material in the presence of interphase boundaries. *Philos. Mag.* **84**(1), 17–28 (2004)
24. Knyazeva, A.G., Grabovetskaya, G.P., Mishin, I.P., Sevostianov, I.: On the micromechanical modelling of the effective diffusion coefficient of a polycrystalline material. *Philos. Mag.* **95**(19), 2046–2066 (2015)
25. Legrand, E., Bouhattate, J., Feaugas, X., Touzain, S., Garmestani, H., Khaleel, M., Li, D.S.: Numerical analysis of the influence of scale effects and microstructure on hydrogen diffusion in polycrystalline aggregates. *Comput. Mater. Sci.* **71**, 1–9 (2013)
26. Oudriss, A., Creus, J., Bouhattate, J., Conforto, E., Berziou, C., Savall, C., Feaugas, X.: Grain size and grain-boundary effects on diffusion and trapping of hydrogen in pure nickel. *Acta Mater.* **60**(19), 6814–6828 (2012)
27. Brass, A.M., Chanfreau, A.: Accelerated diffusion of hydrogen along grain boundaries in nickel. *Acta Mater.* **44**(9), 3823–3831 (1996)

28. Sevostianov, I.: On the shape of effective inclusion in the Maxwell homogenization scheme for anisotropic elastic composites. *Mech. Mater.* **75**, 45–59 (2014)
29. Kachanov, M., Sevostianov, I.: Micromechanics of materials, with applications. In: *Solid Mechanics and Its Applications*, vol. 249. Springer, Cham (2018)
30. Kachanov, M., Sevostianov, I.: On quantitative characterization of microstructures and effective properties. *Int. J. Solids Struct.* **42**(2), 309–336 (2005)
31. Markov, K.Z.: Elementary micromechanics of heterogeneous media. In: Markov, K., Preziosi, L. (eds.) *Heterogeneous Media. Modeling and Simulation in Science, Engineering and Technology*, pp. 1–162. Birkhäuser, Boston, MA (2000)
32. Maxwell, J.C.: *A Treatise on Electricity and Magnetism*. Clarendon Press, Oxford (1873)
33. Rayleigh, L.: LVI. On the influence of obstacles arranged in rectangular order upon the properties of a medium. *Philos. Mag. J. Sci. The London, Edinburgh, and Dublin* **34**(211), 481–502 (1892)
34. Sevostianov, I., Giraud, A.: Generalization of Maxwell homogenization scheme for elastic material containing inhomogeneities of diverse shape. *Int. J. Eng. Sci.* **64**, 23–36 (2013)
35. Belova, I.V., Murch, G.E.: Calculation of the effective conductivity and diffusivity in composite solid electrolytes. *J. Phys. Chem. Solids* **66**(5), 722–728 (2005)
36. Kalnin, J.R., Kotomin, E.A., Maier, J.: Calculations of the effective diffusion coefficient for inhomogeneous media. *J. Phys. Chem. Solids* **63**(3), 449–456 (2002)
37. Frolova, K.P.: Determination of the effective Young's modulus of medium with microstructure typical for hydrogen degradation. *J. Phys. Math. St. Petersburg State Polytechnic University* **13**(2), 160 (2020)